

Particle Acceleration in Supernova Remnants and Pulsar Wind Nebulae

Patrick Slane

*Harvard-Smithsonian Center for Astrophysics
60 Garden Street
Cambridge, MA 02138, USA*

While supernova remnants (SNRs) have long been considered prime candidates for the source of cosmic rays, at least to energies up to $\sim 10^{14}$ eV, it is only over the past several years that direct evidence of such energetic particles in SNRs has been uncovered. X-ray observations of several shell-type SNRs have now revealed sites dominated by nonthermal emission, indicating an electron population whose energy extends far beyond the thermal distribution typical of such SNRs. In other remnants, discrepancies between the shock velocity and the electron temperature points to a strong cosmic ray component that has essentially thrived at the expense of the thermal component of the gas. Modeling of the radio, X-ray, and gamma-ray emission provides strong constraints on the acceleration mechanism as well as the properties of the ambient medium in which the mechanism prospers. In the innermost regions of some SNRs, particle acceleration is taking place over much different scales. The formation of Crab-like pulsar wind nebulae (PWNe) is understood to require the presence of a termination shock at which the relativistic pulsar wind is forced to join the slow expansion of the outer nebula. While the acceleration mechanism is necessarily different, these shocks also act as sites in which particles are boosted to high energies. In the Crab Nebula, optical wisps mark the location of this termination shock. Recent X-ray observations have begun to reveal the termination shock zones in other PWNe, and are now allowing us to constrain the nature of the pulsar wind as well as the flow conditions in the outer nebula. Here I present a summary of the properties of shock acceleration in these two distinct regions of SNRs, and review recent observational results in which the properties of the shocks are finally being revealed.

1 Introduction

Supernova remnants and their associated pulsars are sites in which strong shocks act to accelerate particles to extremely high energies. The connection between SNRs and the energetic cosmic rays that pervade the Galaxy has long been assumed, for example; shock acceleration by the SNR blast wave provides ample energy for the production of multi-TeV particles, and recent observations of nonthermal X-ray and VHE γ -ray emission from several SNRs has confirmed the presence of electrons at these high energies. At the same time, models for the structure of PWNe predict particle acceleration at the wind termination shock, and recent X-ray observations have begun to probe these acceleration sites. Here I review recent and ongoing observational X-ray studies of particle acceleration by shocks in SNRs and PWNe.

2 Shocks and Particle Acceleration in SNRs

The birthrate and overall energetics of SNRs provide a strong plausibility argument that they are a major source of cosmic rays up to the “knee” of the spectrum. However, until recently

the only direct evidence of energetic particles from SNRs has been from the radio synchrotron emission. But this corresponds to electron energies

$$E_{\text{GeV}} \approx \left[\frac{\nu}{16 \text{ MHz}} B_{\mu}^{-1} \right]^{1/2} \quad (1)$$

where ν is the frequency of the radio emission and B_{μ} is the magnetic field strength in micro-Gauss. Thus, while providing a clue, the radio emission samples only electrons far below the cosmic ray knee. X-ray observations allow us to characterize the thermodynamic states of SNRs and to infer the dynamics of their evolution, probing much higher particle energies. As the blast wave from a supernova explosion expands, material from the surrounding circumstellar material (CSM) and ISM is swept up into a shell of hot gas. For an ideal gas, the shock jump conditions yield an increase in density by a factor of 4 and a postshock temperature of

$$T = \frac{3\mu m}{16k} V_s^2 \quad (2)$$

where V_s is the shock speed, m is the proton mass, and μ is the mean molecular weight of the gas ($\mu \approx 0.6$). This shock-heated gas yields the familiar X-ray emission, characterized by a thermal bremsstrahlung spectrum accompanied by strong emission lines. As increasing amounts of material are swept up by the blast wave, the shock is decelerated and the ejecta from the explosion encounter the dense shell. A reverse-shock is generated, heating the ejecta. At early times, then, the X-ray spectrum is dominated by emission from the ejecta. As the amount of swept-up material increases, the spectrum becomes dominated by emission from material with ISM abundances.

In addition to thermal heating of the swept-up gas, some fraction of the shock energy density goes into nonthermal production of relativistic particles through diffusive shock acceleration. The maximum particle energy in such a scenario can be limited by radiative losses, the finite age of the SNR, or particle escape from the accelerating region. Radio observations of SNRs provide ample evidence of electrons with GeV energies through synchrotron radiation in the compressed magnetic field at the remnant shell. At higher particle energies, γ -ray production may result from nonthermal bremsstrahlung of electrons colliding with ambient gas, from inverse Compton scattering of ambient photons, and from the decay of neutral pions created by the collision of energetic protons. If the relativistic particle component of the energy density becomes comparable to that of the thermal component, the shock acceleration process can become highly nonlinear. The gas becomes more compressible, which results in a higher density and enhanced acceleration. When the acceleration is very efficient, the relationship between the shock velocity and the mean postshock temperature is no longer well approximated by Eq. 1; the acceleration process depletes thermal energy, and the temperature for a given shock velocity drops below that expected in the test particle case¹. This process has been considered in detail by Baring et al.² who present a model for the radio to γ -ray emission. The broadband spectra of SNRs depend highly on ambient conditions, and X-ray studies of these SNRs reveal these conditions and can provide spectral measurements which strongly constrain the models.

In the simplest picture, the passage of material through the SNR shock results in electrons and ions being boosted to the velocity of the shock. Because of the mass difference, this means that the electrons and ions are not initially in temperature equilibrium. The maximum timescale for equilibration is that provided by Coulomb interactions, but plasma processes may reduce this considerably. The state of equilibration is important, because while the dynamics of SNR evolution are dominated by the ions (which carry the bulk of the momentum), it is the electrons that produce the X-ray emission we observe. Thus, when temperature measurements are used to infer the shock velocity, for example, the state of temperature equilibration is exceedingly important. *Chandra* HETG observations of SN 1987A,³ for example, yield spectra consistent

with an electron temperature of 2.6 keV. However, the broadened line profiles indicate a blast wave speed of $\sim 3500 \text{ km s}^{-1}$ which corresponds to a post-shock temperature of 17 keV, providing evidence for incomplete electron-ion temperature equilibration. Similarly, the blast wave speed inferred from an expansion study comparing a *Chandra* image of 1E 0102.2–7219 with high resolution images taken with *Einstein* and *ROSAT* indicates a post-shock temperature which is much higher than the observed electron temperature.⁴ In this case, the discrepancy appears to be larger than can be accounted for assuming Coulomb equilibration, suggesting that a significant fraction of the shock energy has gone into cosmic ray acceleration rather than thermal heating of the postshock gas. Higher resolution X-ray expansion studies of 1E 0102.2–7219 (and other young SNRs) are needed to confirm this scenario, but the notion that particle acceleration is efficient enough in some SNRs to significantly affect their dynamics has strong foundations from recent studies of other SNRs. As we discuss below, direct evidence of very energetic electrons now exists for a handful of shell-type SNRs. In addition to the three SNRs which we discuss in the following sections, for which synchrotron radiation dominates the X-ray emission, evidence for energetic particles in the form of hard tails in the X-ray spectra have also been observed for Cas A^{5,6} RCW 86,^{7,8} and other SNRs.

2.1 SN 1006

The first evidence of multi-TeV particles directly associated with a shell-type SNR was uncovered in studies of SN 1006 with the ASCA observatory.⁹ While spectra from the central regions of the SNR show distinct line emission associated with shock-heated gas, the emission from the bright limbs of the remnant was shown to be completely dominated by synchrotron emission. Reynolds¹⁰ modeled the emission as the result of diffusive shock acceleration in a low density medium with the magnetic field orientation providing the distinct “bilateral” morphology. Subsequent observations with the CANGAROO telescope revealed VHE γ -ray emission from one limb of the SNR,¹¹ thus confirming the presence of extremely energetic particles. The low ambient density of this remnant, which resides well above the Galactic Plane, is insufficient to explain the γ -ray emission as the result of π^0 decay from proton-proton collisions. Rather, the emission results from inverse-Compton scattering of microwave background photons off the energetic electron population in SN 1006. Using joint spectral fits to the radio as well as thermal and nonthermal X-ray emission, Dyer et al.¹² conclude that the total energy in relativistic particles is ~ 100 times the energy in the magnetic field, confirming the notion that the nonthermal particle component contributes significantly to the dynamics of the blast wave evolution.

2.2 G347.3–0.5 (RX J1713.7–3946)

ASCA observations of G347.3–0.5^{13,14} established this as the second member of the class of shell-type SNRs for which the X-ray flux is dominated by synchrotron radiation. Unlike SN 1006, this SNR appears to have evolved in the vicinity of dense molecular clouds¹⁴ with which the shock may now be interacting. CANGAROO observations¹⁵ reveal VHE γ -ray emission from the vicinity of the northwest rim, which is brightest in X-rays. Combining radio measurements from the ATCA with the X-ray and γ -ray results, Ellison, Slane, & Gaensler¹⁶ used diffusive shock acceleration models to conclude that the radio and X-ray emission results from synchrotron radiation from a nonthermal electron population accelerated by the forward shock, and that the γ -ray emission can be self-consistently modeled as inverse-Compton emission (Figure 1). Combined with limits on the ambient density based on the lack of thermal X-ray emission, the models indicate very efficient particle acceleration with $> 25\%$ of the shock kinetic energy going into relativistic ions. A comparison of *Chandra* observations of the northwest rim with high resolution radio maps from the ATCA shows good overall agreement with the radio and X-ray

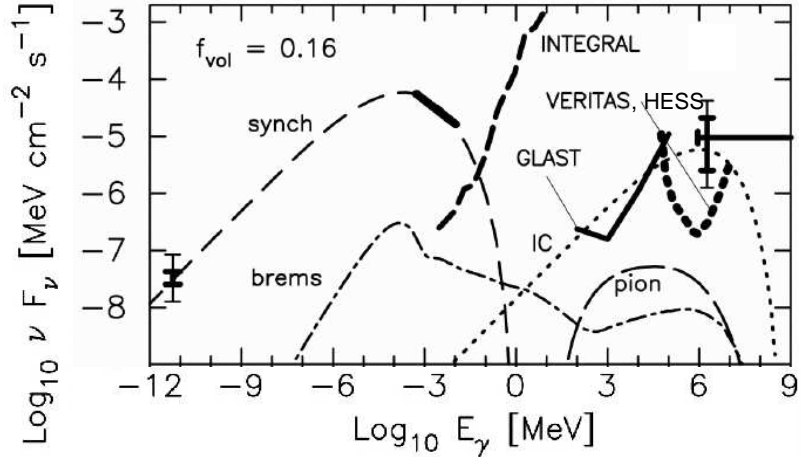


Figure 1: Comparison of broadband emission from the northwest limb of G347.3-0.5 with diffusive shock acceleration model results (from Ellison, Slane, & Gaensler 2001). The radio and X-ray emission is from synchrotron radiation while the VHE γ -ray emission is from inverse-Compton scattering. Sensitivities of future high energy telescopes are shown for comparison.

morphology in this region (Figure 2), consistent with the interpretation that the emission comes from the same electron population.¹⁷

The nearby unidentified EGRET source 3EG J1714-3857 has been suggested as being associated with G347.3-0.5, possibly resulting from the decay of neutral pions produced in the collision of accelerated ions with the nearby molecular clouds,¹⁸ although this would appear inconsistent with the X-ray measurements unless the emission originates from a distinct spatial region. Most recently, Enomoto et al.¹⁹ present new CANGAROO data which, they argue, establishes π^0 -decay as the mechanism by which the TeV γ -rays are produced. However, the predicted spectrum overpredicts emission from the EGRET band by a large margin,²⁰ making the claim for direct observation of ion acceleration appear problematic.

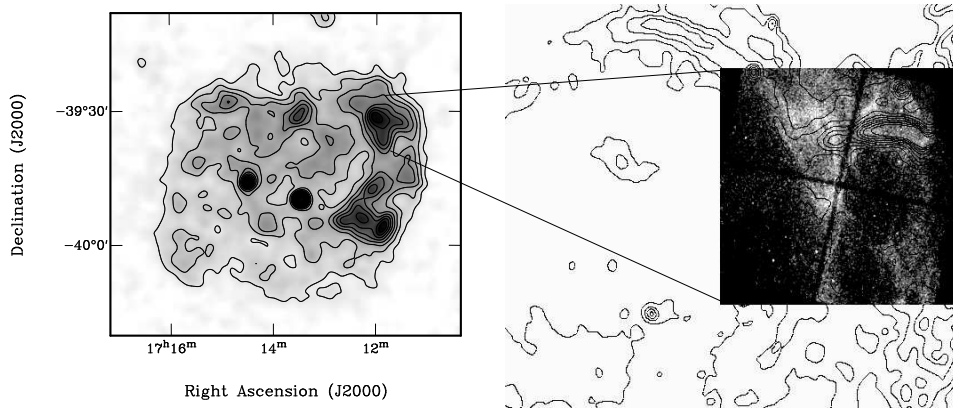


Figure 2: Left: ROSAT PSPC image of G347.3-0.5. Right: *Chandra* image of northwest rim of G347.3-0.5, with radio contours from ATCA.

2.3 G266.2-1.2 (RX J0852.0-4622)

G266.2-1.2 is an SNR lying along the line of sight to the southeast corner of the Vela SNR. Discovered in the ROSAT All-Sky Survey,²¹ the remnant is evident only at higher X-ray energies where the very soft spectrum of Vela does not contribute. ASCA observations²² show that the

X-ray emission from this remnant is also predominantly synchrotron radiation. To date, no high energy γ -ray emission has been reported for this remnant, although there have been claims of ^{44}Ti line emission²³ which, given the very short half-life, would require an extremely young age. The radio flux from G266.2–1.2 is extremely low,²⁴ much like that of SN 1006 and G347.3–0.5. The overall properties of this remnant are indicative of efficient shock acceleration of particles to very high energies, but further investigations are required to quantify the dynamics.

3 Energetic Particles from Pulsars and Their Wind Nebulae

Our basic understanding of “Crab-like” SNRs stems from the picture presented by Rees & Gunn²⁵, and expanded upon by Kennel & Coroniti,^{26,27} in which an energetic wind is injected from a pulsar into its surroundings. As illustrated schematically in Figure 3, the basic structure of a pulsar wind nebula is regulated by the input power from the pulsar and the density of the medium into which the nebula expands; the pulsar wind inflates a magnetic bubble which is confined in the outer regions by the expanding shell of ejecta or interstellar material swept up by the SNR blast wave. The boundary condition established by the expansion at the nebula radius r_N results in the formation of a wind termination shock at which the highly relativistic pulsar wind is decelerated to $v \approx c/3$ in the postshock region, ultimately merging with the particle flow in the nebula. The shock forms at the radius r_w at which the ram pressure of the wind is balanced by the internal pressure of the pulsar wind nebula:

$$r_w^2 = \dot{E}/(4\pi\eta cp) \quad (3)$$

where \dot{E} is the rate at which the pulsar injects energy into the wind, η is the fraction of a spherical surface covered by the wind, and p is the total pressure outside the shock.

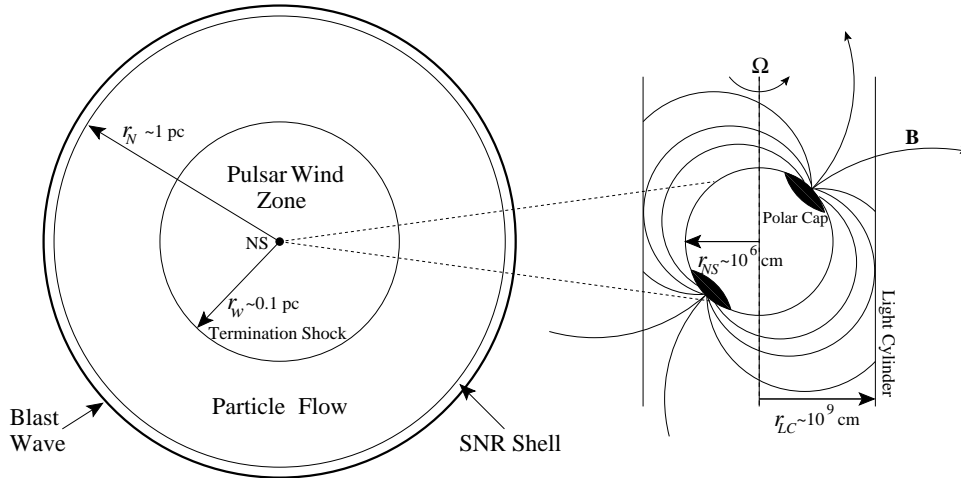


Figure 3: Schematic view of a pulsar and its wind nebula. See the text for a complete description. (Note the logarithmic size scaling in the PWN figure when comparing with images shown elsewhere in the text.)

The dynamics of the particle flow yield $\gamma \sim 10^6$ for the electrons in the postshock region.²⁸ However, for typical magnetic field strengths the observed X-ray emission requires $\gamma > 10^8$. Particle acceleration at the termination shock apparently boosts the energies of the wind particles by a factor of 100 or more, to energies in excess of ~ 50 TeV. Arons & Tavani²⁸ (see also Arons²⁹) note that this process cannot proceed by normal diffusive shock acceleration because the magnetic field at the termination shock must be nearly perpendicular to the flow. Rather, they argue that the e^\pm acceleration is the result of resonant cyclotron absorption of low frequency electromagnetic waves emitted by ions gyrating in the compressed B -field of the hot post-shock

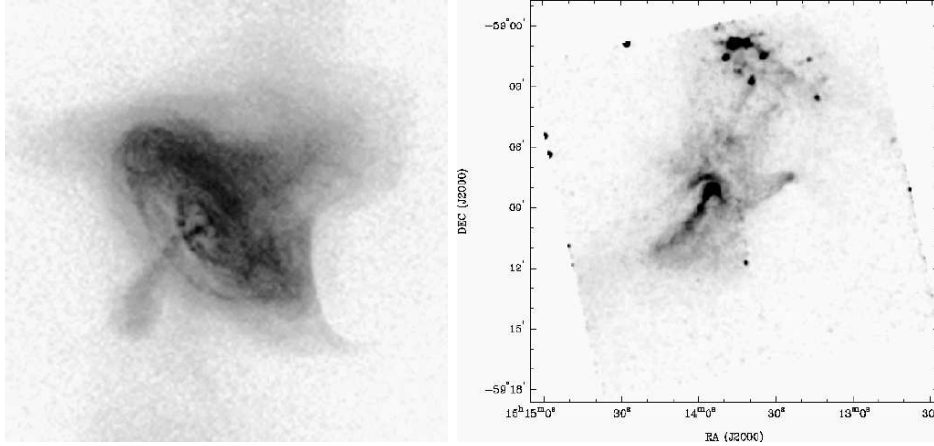


Figure 4: *Chandra* image of the Crab Nebula (left) and the pulsar wind nebula associated with PSR B1509–58 (right; image courtesy of B. Gaensler).

gas. Ultimately, the pressure in the nebula is believed to reach the equipartition value; a reasonable pressure estimate can be obtained by integrating the radio spectrum of the nebula, using standard synchrotron emission expressions, and assuming equipartition between particles and the magnetic field. Typical values yield termination shock radii of order 0.1 pc, which yields an angular size of several arcsec at distances of a few kpc.

The magnetic field in the PWN builds up with radius as the result of particle currents and wound-up magnetic flux from beyond the pulsar light cylinder at $r_{LC} = c/\Omega$. The finite lifetime of the synchrotron-emitting particles in the nebula,

$$t_{syn} \approx 5 \times 10^{11} / (B^{3/2} \nu^{1/2}) \text{ s}$$

(where ν is the frequency of the synchrotron radiation), results in fewer high energy particles at large radii. This manifests itself as a variation of the nebula radius with energy (which is clearly seen in the Crab Nebula, for which the radio size is larger than that seen in X-rays) or, equivalently, as a radial variation in the X-ray spectrum, with the power law index steepening with radius.

The pulsar wind can be characterized in terms of \dot{E} and the parameter σ representing the ratio of Poynting flux to particle flux. For the Crab Nebula, Kennel & Coroniti²⁶ find that small values of σ ($\sim 10^{-3}$) are required, indicating a particle-dominated wind. Yet current understanding of pulsar outflows predicts $\sigma \gg 1$ where the wind is launched.²⁹ Somehow, between the pulsar light cylinder and the wind termination shock the balance between the electromagnetic energy and the kinetic energy of the flow changes dramatically. The ability to identify the termination shock and measure the emission parameters in the immediate region is now providing constraints on the nature of the wind that may ultimately help unravel this problem. Below I summarize recent X-ray investigations that have finally begun to probe this important shock region in which particle acceleration is apparently taking place.

3.1 Crab Nebula

The Crab Nebula is the best known of the class of pulsar wind nebulae and has inspired much of the theoretical work on PWNe. Powered by an energetic central pulsar, it emits synchrotron radiation from radio wavelengths up beyond the hard X-ray band. Optical wisps are observed in the inner nebula, at a position interpreted as the pulsar wind termination shock,³⁰ and high resolution X-ray observations (Figure 4, left) reveal a distinct ring of emission in this same region as well as a jet emanating from the pulsar.³¹ Moreover, monitoring observations of the

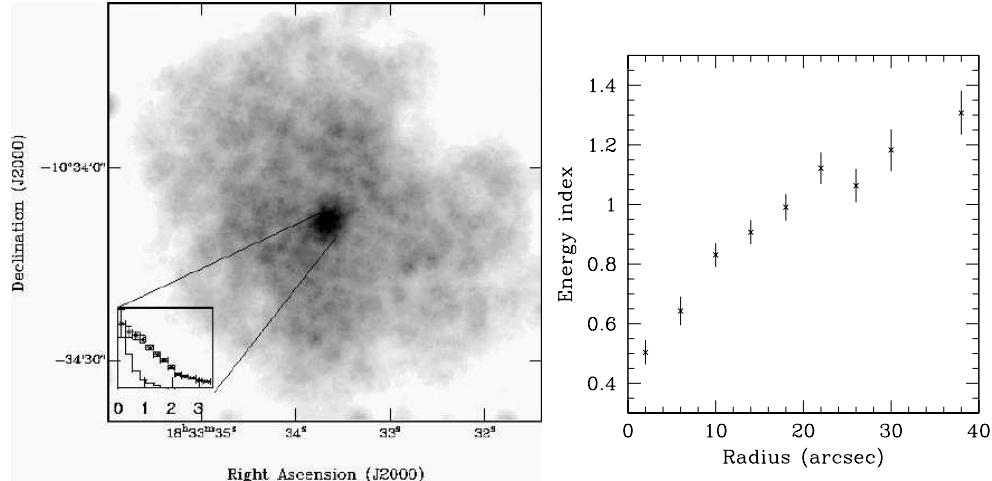


Figure 5: Left: *Chandra* image of G21.5-0.9. The inset shows the brightness profile of the compact central region compared with a histogram of that from a point source in the telescope. Right: Spectral index variation with radius in the nebula, indicating the synchrotron burn-off of particles injected at the center of the nebula.

Nebula^{30,32} show that these and other detailed features are highly dynamic. The discovery of radio wisps in inner ring region³³ suggests that the acceleration site may be the same for the entire population of electrons that produce the broad-band synchrotron emission.

In addition to the jet and inner ring, the X-ray image reveals an outer toroidal structure that presumably lies in the equatorial plane, as well as fine structure correlated with optical polarization measurements, indicating that the structures trace the magnetic field. The early models of Rees & Gunn²⁵ and Kennel & Coroniti^{26,27} predict these basic properties as the result of a wound-up magnetic field, the large-scale confinement of the Nebula by the (unseen) supernova ejecta, and the termination of the pulsar wind flow by an inner shock. This picture leads to the inference of a low- σ wind described above. As we describe below, recent observations of PWNe have begun to show many similar features, indicating that our basic picture – while still poorly understood in detail – can at least be said to apply to a “class” of objects.

3.2 PSR B1509–58

The PWN powered by the energetic young pulsar B1509–58 (Figure 4, right) displays a complex morphology rivaling that of the Crab Nebula. *Chandra* observations³⁴ reveal a clear symmetry axis, presumably corresponding to the pulsar spin axis, with an apparent curved jet along this axis. Arc-like features in the inner nebula appear to correspond to equatorial structures similar in nature and origin to the wisps seen inside the Crab X-ray torus. Gaensler et al.³⁴ show that $\sigma \sim 0.005$ at these wisps, with other compact knots seen very close to the pulsar indicating even smaller σ values upstream of the wind shock zone. The PWN has a much weaker magnetic field than the Crab, and synchrotron losses affect the spectra of outflowing particles only at large radii. The hard spectra observed for the compact knots suggest a different acceleration mechanism than for larger features, downstream of the termination shock. In the northernmost regions of the PWN, clumps of thermally-emitting gas from the associated SNR appear to be embedded in the nebula.

3.3 G21.5–0.9

G21.5–0.9 is a compact SNR that exhibits strong linear polarization, a flat spectrum, and centrally peaked emission in the radio band. The SNR has a lower L_x/L_r ratio than the Crab; it is a factor of ~ 9 less luminous in the radio and a factor of ~ 100 less in X-rays. To date,

there has been no detection of a central pulsar. However, *Chandra* observations by Slane et al.³⁵ reveal a compact source of emission at the center of the remnant as well as a radial steepening of the spectral index consistent with synchrotron burn-off of high energy electrons injected from a central source (Figure 5). Using an empirical relationship between the total X-ray luminosity of the PWN with the spin-down power of the pulsar powering the nebula³⁶ suggests the presence of a pulsar with $\dot{E} = 10^{37.5}$ erg s⁻¹, although Chevalier³⁷ argues that the spectral variations in the nebula imply more efficient conversion of \dot{E} into X-ray emission, and suggests that $\dot{E} \approx 10^{36.7}$ erg s⁻¹ is more likely for the pulsar in this PWN. Detection of pulsations from the central source are required to address this further. Using the larger \dot{E} estimate along with pressure estimates from the radio spectrum, Eq. 3 predicts a wind termination shock at a radius of $\sim 1.5\eta^{-1/2}$ arcsec from the pulsar, assuming a distance of 5 kpc. As indicated in the inset to Figure 5, the brightness profile of the compact X-ray source in G21.5–0.9 is broader than that for a point source. The $\sim 2''$ extent of the source is consistent with the expected size of the termination shock zone. The small radius of the termination shock combined with the large radius of the PWN yields $\sigma \ll 1$; as with the Crab, the pulsar wind is particle-dominated in the termination shock zone.

Slane et al.³⁵ also report the presence of a faint extended shell of emission surrounding G21.5–0.9 whose featureless spectrum may be associated with energetic particles accelerated by the SNR blast wave, similar to those observed for SN 1006 and other SNRs as described in Section 2. Safi-Harb et al.³⁸ and Warwick et al.³⁹ confirm the presence of the shell, but suggest that it is a faint extension of the PWN, though no extended radio shell is observed.

3.4 3C58

3C58 (Figure 6, left) is a young Crab-like supernova remnant. Historical evidence strongly suggests an association of the remnant with supernova SN 1181, which would make 3C58 younger than the Crab Nebula. Recent *Chandra* observations have identified the young 65 ms pulsar J0205+6449 at its center,⁴⁰ embedded in a compact nebula which appears to be confined by the pulsar wind termination shock.⁴¹ The central region of 3C58 is shown in Figure 5 (center). The emission is clearly extended, with elongation in the N-S direction, perpendicular to the long axis of the main nebula; the full extent in this direction is $\sim 25''$. PSR J0205+6449 resides at the center of this compact nebula.

The western edge of the compact nebula lies directly along a radio filament,⁴² shown as contours in Figure 5 (center), and there appears to be a slight flattening of compact nebula along this side. Frail & Moffett⁴² suggested that this filament may represent the position of the termination shock where the pulsar wind is confined by the interior pressure of the PWN. Adopting the generally accepted distance $d = 3.2d_{3.2}$ kpc, integration of the radio synchrotron spectrum yields a pressure of $P_{\text{neb}} = 3.2 \times 10^{-10} d_{3.2}^{-1}$ dyne cm⁻² under the assumption of equipartition between the electron and magnetic energy densities. The spin-down properties of the pulsar give $\dot{E} = 2.6 \times 10^{37} I_{45}$ erg s⁻¹ where I_{45} is the NS moment of inertia in units of 10^{45} gm cm². Ram pressure balance should thus occur at $r_w = 5.5 \times 10^{17} I_{45}^{1/2} \eta^{-1/2} d_{3.2}^{1/2}$ cm, or at an angular distance $\theta = 11.4 I_{45}^{1/2} \eta^{-1/2} d_{3.2}^{-1/2}$ arcsec. This is in good agreement with the the ~ 12 arcsec radial extent of the core X-ray emission in the NS direction, suggesting that the compact nebula surrounding the pulsar is bounded by the pulsar wind termination shock. It is possible that this is actually a toroidal structure, much like that seen in the Crab Nebula, and that the elongated surface brightness distribution is the result of the inclination angle. In this interpretation, the axis of the toroid, which presumably lies along the rotation axis of the pulsar, lies in the east-west direction when projected onto the sky. We note that the long axis of 3C58 itself, as well as an extended jet-like feature shown in Figure 5 (right), are both aligned in this direction. Assuming that the radio filament lies along one side of the torus, its separation from the pulsar

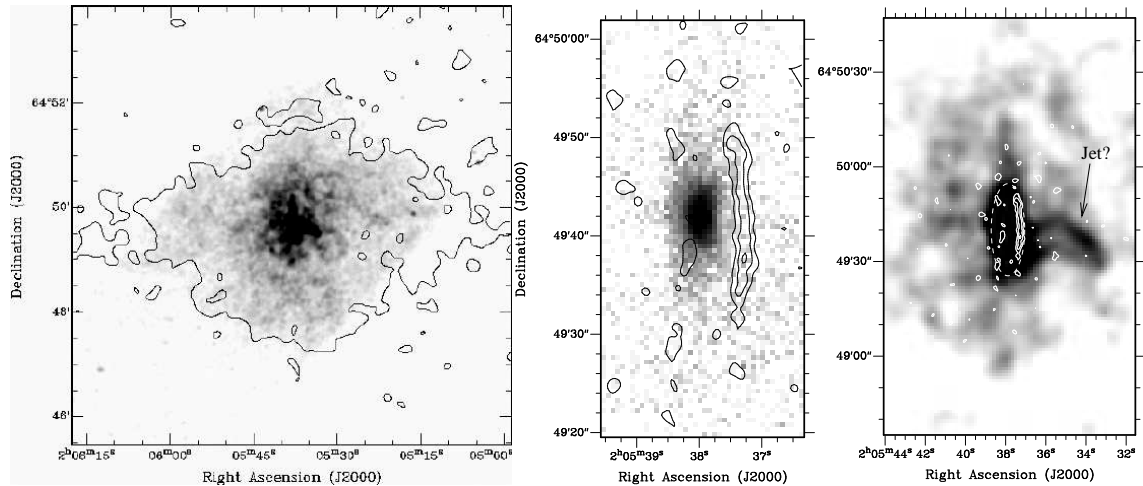


Figure 6: Left: ACIS image of 3C 58. Some portions of the nebula extend beyond the detector boundary, as indicated by the outermost contour from the HRC image, which is superposed. Center: ACIS image of the central region of 3C 58, with contours from 20 cm VLA data showing a faint radio wisp that bounds the X-ray core. Right: Saturated image of 3C 58 core, on a larger scale, revealing the faint jetlike feature extending toward the west. The dashed ellipse indicates the rough outline of the extended X-ray core.

(~ 4.5 arcsec) implies an inclination angle of $\sim 70^\circ$.

4 Summary

The strong shocks in SNRs and pulsar wind nebulae have long been regarded as sites where particles are accelerated to extremely high energies. SNRs, in particular, are leading candidates as the source of cosmic rays up to the knee of the spectrum. X-ray emission from PWNe also require particles with higher energies than expected in the postshock flow of the pulsar wind, indicating efficient acceleration at the termination shock. X-ray observations have now begun to provide direct evidence of the energetic particles and shock structures where this such acceleration takes place. Through studies of the dynamics and nonthermal X-ray emission from the shells of SNRs, and of the location and structure of the wind termination shocks and associated particle outflows in PWNe, strong constraints are being placed on models of the particle acceleration process. High resolution X-ray observations promise continued advances in this area, through measurements of SNR nonthermal emission and expansion rates, and the inner structure of PWNe. In addition, γ -ray observations with current and upcoming Čerenkov telescopes, as well as future space-borne observatories, hold considerable promise for probing these sites of extremely energetic particles.

Acknowledgments

The author would like to thank Bryan Gaensler, Jack Hughes, and Don Ellison for their contributions as collaborators on much of the above work. This research was funded in part by NASA Contract NAS8-39073 and Grants NAG5-9281 and GO0-1117A.

References

1. Decourchelle, A., Ellison, D. C., & Ballet, J. 2002, ApJ 543, L57.
2. Baring, M. G. et al. 1999, ApJ, 513, 311
3. Michael et al. 2002, ApJ - in press (astro-ph/0112261)

4. Hughes, J. P., Rakowski, C. E. & Decourchelle, A. 2001, *ApJ*, 543, L61
5. Allen, G. E. et al. 1997, *ApJ*, 487, L97
6. Vink, J. et al. 1999 *A&A*, 344, 289
7. Allen, G. E., Gotthelf, E. V., & Petre, R. 1999, Proc. 26th Int. Cosmic Ray Conf. (Salt Lake City), 3, 480
8. Borkowski et al. 2001, *ApJ*, 550, 334
9. Koyama, K. et al. 1995, *Nature*, 378, 255
10. Reynolds, S. P. 1998, *ApJ*, 493, 375
11. Tanimori, T. et al. 1998, *ApJ*, 497, L25
12. Dyer, K. K. et al. 2001, *ApJ*, 551, 439
13. Koyama, K. et al. 1997, *PASJ*, 49, L7
14. Slane, P. et al. 1999, *ApJ*, 525, 357
15. Muraishi, T. et al. 2000, *A&A*, 354, L57
16. Ellison, D. C., Slane, P., & Gaensler, B. M. 2001, *ApJ*, 563, 191
17. Lazendic, J. et al. 2002 - in preparation
18. Butt, Y., et al. 2001, *ApJ*, 562, L167
19. Enomoto, R. et al. 2002, *Nature*, 416, 823
20. Reimer, O. et al. 2002, *A&A* - submitted (astro-ph/0205256)
21. Aschenbach, B. 1998, *Nature*, 396, 141
22. Slane, P. et al. 2001, *ApJ*, 548, 814
23. Iyudin, A. F., et al. 1998, *Nature*, 396, 142
24. Duncan, A. R. & Green, D. A. 2000, *A&A*, 364, 732
25. Rees, M. J. & Gunn, R. E. 1974, *MNRAS*, 167, 1
26. Kennel, C. F. & Coroniti, F. V. 1984, *ApJ*, 283, 694
27. Kennel, C. F. & Coroniti, F. V. 1984, *ApJ*, 283, 710
28. Arons, J. & Tavani, M. 1994, *ApJS*, 90, 797
29. Arons, J. 2002, to appear in "Neutron Stars in Supernova Remnants" (ASP Conference Proceedings), eds P. O. Slane and B. M. Gaensler
30. Hester, J. J. et al. 1995, *ApJ*, 448, 240
31. Weisskopf, M. C. et al. 2000, 536, L81
32. Mori, K. et al. 2002, to appear in "Neutron Stars in Supernova Remnants" (ASP Conference Proceedings), eds P. O. Slane and B. M. Gaensler
33. Bietenholz, M. F., Frail, D. A., & Hester, J. J. 2001, *ApJ*, 560, 254
34. Gaensler, B. M. et al. 2002, *ApJ*, 569, 878
35. Slane, P. et al. 2000, *ApJ*, **533**, L29
36. Seward, F. D. & Wang, Z.-R. 1988, *ApJ*, 332, 199
37. Chevalier, R. A. 2000, *ApJ*, 539, L45
38. Safi-Harb, S. et al. 2001, *ApJ*, 561, 308
39. Warwick, R. S. et al, *A&A*, 365, L248
40. Murray, S. S. et al. 2001, *ApJ*, 68, 226
41. Slane, P. O., Helfand, D. J., & Murray, S. S. 2002, *ApJ*, 571, L45
42. Frail, D. A., & Moffett, D. A. 1993, *ApJ*, 408, 637